Available online at www.sciencedirect.com
ScienceDirect
Journal of the European Ceramic Society 31 (2011) 469–474
www.elsevier.com/locate/jeurceramsoc

Dry reciprocating sliding wear behaviour of alumina–silicon carbide nanocomposite fabricated by ceramic injection molding

A. Smirnov [a,1], J.F. Bartolomé [a,*], J.S. Moya [a], F. Kern [b], R. Gadow [b]

[a] *Instituto de Ciencia de Materiales de Madrid (ICMM), Consejo Superior de Investigaciones Científicas (CSIC), C/Sor Juana Inés de la Cruz 3, 28049 Madrid, Spain*

[b] *Institut für Fertigungstechnik keramischer Bauteile (IFKB), Universität Stuttgart, Allmandring 7B, D-70569 Stuttgart, Germany*

Received 17 March 2010; received in revised form 22 October 2010; accepted 2 November 2010
Available online 3 December 2010

Abstract

The wear resistance of Al_2O_3 composite with 6 vol.% of SiC nanoparticles fabricated by thermoplastic forming technology and natural sintering was studied under reciprocating dry sliding conditions and compared with the results obtained in unreinforced alumina with similar grain size obtained by hot pressing. The nanocomposite wear resistance at contact loads of 20 N corresponding to initial Hertzian contact pressures of 1.8 GPa, was found to be superior to that of the alumina by a factor of 6.

Keywords: Al_2O_3–SiC; Injection molding; Mechanical properties; Wear resistance

1. Introduction

Experiments carried out by many researchers[1,2] have shown that the mechanical properties and wear of alumina can be significantly enhanced by the dispersion of ceramic particles in the nanometer size range. Several mechanisms have been proposed for the enhancement of the mechanical properties (strength and toughness) of nanocomposites; these include thermal residual stresses, change in grain boundary morphology, dislocation activity, enhanced interfacial fracture energy, etc.[3]

However, the most remarkable and reliable benefit offered by nanocomposites is in their tribological properties. In recent works, for Al_2O_3–SiC nanocomposites, significant improvements of the resistance to severe wear and surface finish following grinding and polishing have been reported,[4–15] compared with pure alumina. These nanocomposites tend to exhibit a surface covered in plastic deformation grooves, while for the same severe wear conditions, the monolithic exhibits intergranular fracture. Commercial applications require performing and reliable manufacturing technologies. Recent works[16–21] demonstrate the feasibility of pressureless sintering to fabricate dense alumina–SiC composites by using an affordable recipe for cold isostatic pressed alumina–SiC starting from submicrometric α-alumina and α-SiC powders and using MgO and Y_2O_3 as a densification aids. However, the addition of densification aids may reduce the creep resistance of these materials due to the formation of intergranular glassy phase at high temperature, i.e. 1700 °C. Ceramic injection molding (CIM) was chosen for the production of small and complex shaped components with narrow dimensional tolerances used in engineering applications. For axially symmetric, elongated component geometries such as tubes or rods, thermoplastic extrusion is a more appropriate forming technology. Moreover, as far as we know, there is no technology routine yet adopted for mass production of components.

The purpose of the present work is to analyze the feasibility of the near net shape manufacturing approach using thermoplastic processing technologies in producing high sliding wear resistance Al_2O_3–SiC nanocomposites.

2. Experimental procedure

2.1. Materials processing

The starting powders chosen were AKP30 α-alumina (Sumitomo, Japan, BET specific surface area of 7–9 m^2/g and

* Corresponding author. Tel.: +34 91 3348 996; fax: +34 91 372 0623.
E-mail address: jbartolo@icmm.csic.es (J.F. Bartolomé).
[1] Present address: Department of Materials Engineering, Tallinn University of Technology, Ehitajate tee 5, 19086 Tallinn, Estonia.

0955-2219/$ – see front matter © 2010 Elsevier Ltd. All rights reserved.
doi:10.1016/j.jeurceramsoc.2010.11.003

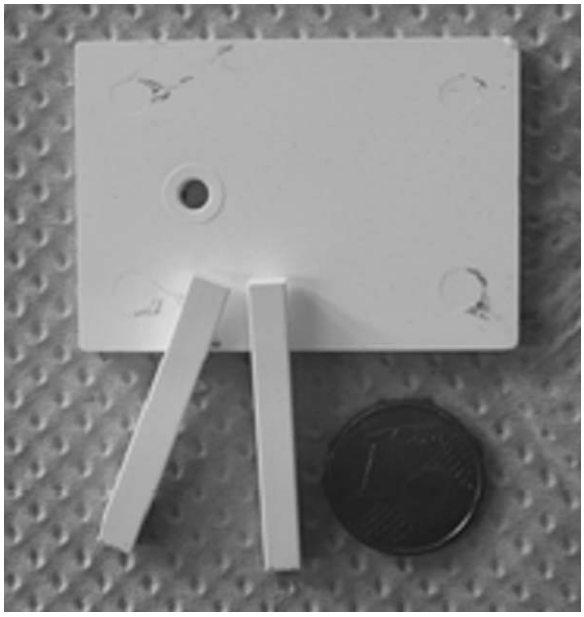

Fig. 1. Injection molded samples.

average particle size of $d_{50} = 0.4\ \mu m$) and UF25 α-silicon carbide (HC Starck, Germany), BET specific surface area of 25 m^2/g and $d_{50} = 450$ nm). Alumina and silicon carbide powders were blended in a weight ratio of 95/5% (93.9/6.1 vol.%). A thermoplastic feedstock consisting of 85 wt.% of the powder blend and 15 wt.% of commercial polyethylene wax binder (Licomont 583 G, Clariant, Germany) were mixed in a double sigmablade kneader (Hermann Linden Maschinenfabrik, Germany) at 140 °C for 1 h. This feedstock was subsequently granulated and homogenized by remelting and mixing in a twin screw extruder ($d = 16$ mm, $L/d = 25$, Haake Rheomex, Thermofisher Scientific, Karlsruhe, Germany) at the same temperature. After the extrusion through a $d = 3$ mm die, cooling and crushing the feedstock was ready for further processing. Rheological characterization was performed by capillary rheometry in the same extruder. The feedstock was extruded through instrumented capillary dies of $d = 2$ mm, $L/d = 10$, 15, 20. The pressure drop along the capillary length and the volumetric flow were measured in the typical processing temperature range of the binder between 130 and 160 °C. The injection molding process was carried out on a hydraulic injection molding machine (Boy50M, Dr. Boy, Germany). Bars (4 mm × 3 mm × 35 mm) and plates (35 mm × 45 mm × 3 mm) were obtained (Fig. 1). Plates with weld lines were produced to determine the strength of weld lines by inserting a pin into the mold at a distance of 10 mm from the gate. Molding parameters were the following: plastification temperature 150–160 °C, mold temperature 60–70 °C, pressure 1000–1200 bar and injection speed 10–30 cm^3/s, the packing pressure was 300-500 bar. The specimens were cooled for 10–20 s before ejection. The machine was manually operated. Debinding of the samples was performed in a combined process following the binder manufacturer's specifications. After extraction of up to 45 mass% of the binder in distilled water at 60 °C overnight, the samples were dried at the same temperature. The remaining binder was thermally removed, the maximum heat treatment temperature of the debinding process in air was limited to 600 °C/3 h to avoid oxidation of the silicon carbide, but remove residual carbon. The debinded samples were subsequently sintered in Argon atmosphere in a kiln with molybdenum lining on alumina supports (Xerion, Freiberg, Germany). Sintering temperature was 1770 °C, soaking time was 3 h each, the heating rate was 2 °C/min and the cooling rate to room temperature was 20 °C/min. For comparison purpose we have also studied a monolithic alumina obtained by Hot Press at 1500 °C during 1 h, starting from α-alumina powder (99.99%) (TM-DAR, Taimei Chemicals Co., Ltd.), with an average particle size of $d_{50} = 0.15\ \mu m$ and a BET specific surface area of 14.5 m^2/g. The bulk densities of all the materials were measured using the Archimedes method.

2.2. Materials characterization

For mechanical characterization the tensile surface of each bar was gently ground with 15 μm, grinding wheels and polished with 6 μm, 3 μm and 1 μm diamond suspension (PHOENIX BETA grinder/polisher with a VECTOR power head, Buehler, UK).

The microstructure of sintered specimens was studied on fracture surfaces by Scanning Electron Microscopy (FE-SEM, FEI Nova NANOSEM 230).

The Vickers hardness, Hv, was measured using a Vickers diamond indenter (Leco 100-A, St. Joseph, MI) on polished surfaces, with applied load of 9.8 N with an indentation time of 10 s. The magnitude of the Vickers hardness was determined according to,

$$\mathrm{Hv} = 1.854\frac{P}{d^2}$$

where P is the applied load (in N) and d is the diagonal length (in m).

The fracture toughness was calculated using the formula given by Miranzo and Moya.[22] The corresponding indentations sizes were determined using an optical microscope (Leica DMRM, Cambridge, UK).

The bending strength was determined using prismatic bars with 3.2 mm width, 30 mm length and 2.4 mm thickness by three-point bending test. The tests were performed according DIN EN 6872 at room temperature using a universal testing machine (Hegewald & Peschke, Germany). The specimens were loaded to failure with a crosshead speed of 0.5 mm/min and a span of 16 mm.

2.3. Wear test set-up and conditions

The dry sliding wear behaviour of the samples was evaluated with a tribometer *Microtest MT/60/NI* in which a pure alumina ball with 3 mm diameter was reciprocally slid against the different materials in conformity with ASTM G133. The applied load (F_N) was 20 N corresponding to initial Hertzian contact pressures of 1.8 GPa. This load was chosen in order to be located in the transition region near severe wear for the monolithic alumina to analyze the differences between the wear behaviour of

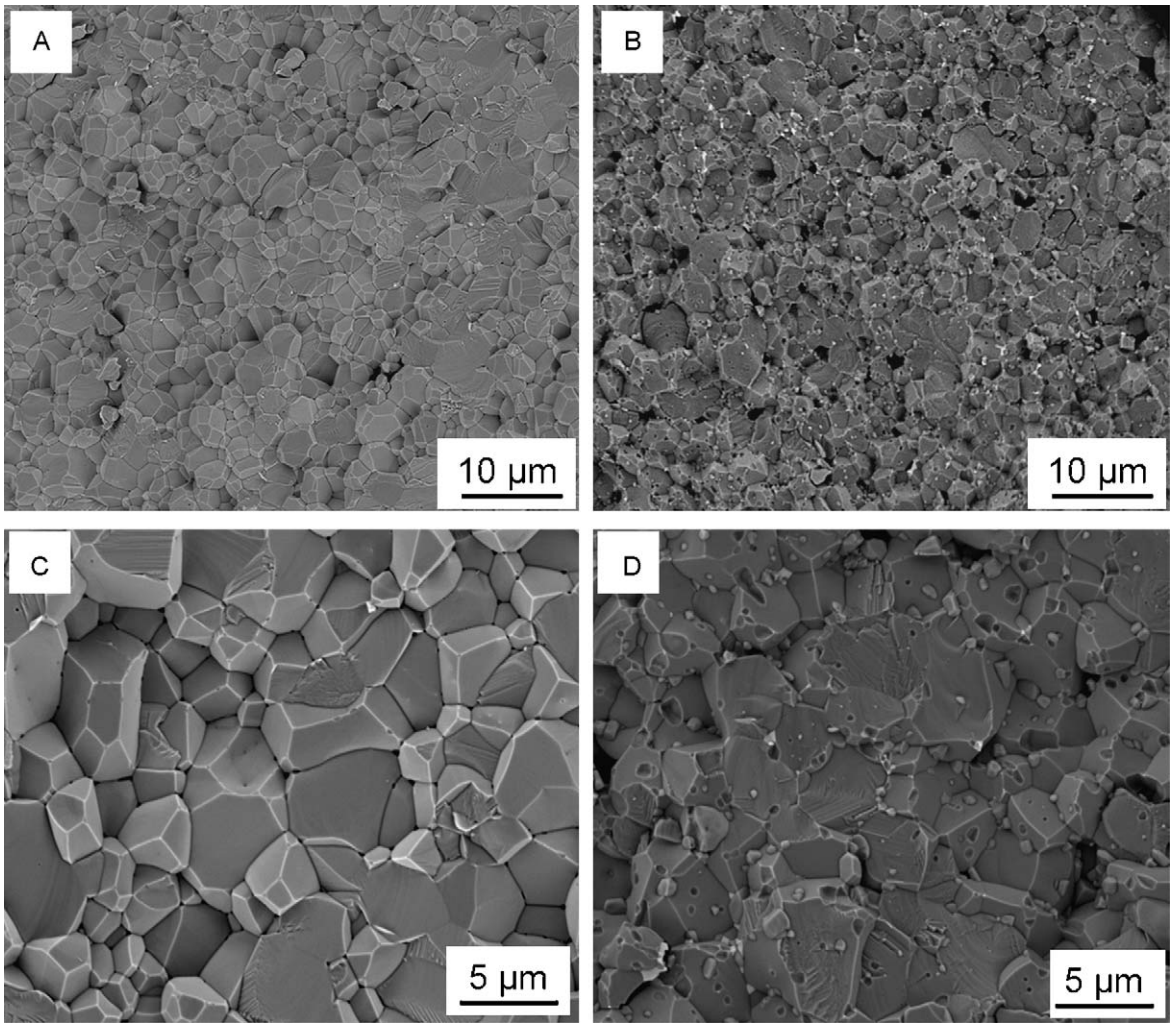

Fig. 2. SEM images of a fracture surface of monolithic Al_2O_3 (A and C) and the Al_2O_3–SiC nanocomposites (B and D).

the monolithic material and that of the nanocomposites, which do not exhibit a time-dependent wear transition.[23] The stroke length of the oscillating motion was 10 mm. A sliding velocity of 0.06 m/s was applied. The test duration was associated with a travelling distance (S) of 10 km. At least 4 sliding wear tests were conducted from each composition. Before each test, the specimens were rinsed ultrasonically in acetone. After each sliding test, the worn surfaces were cleared by blowing pressurized air before post-mortem observations. All tests were performed under the same conditions.

The wear rate was calculated by using Eq. (1):

$$W = \frac{\Delta V}{F_N S} \quad (1)$$

Being ΔV the volume loss after the tests (mm^3), F_N the applied load (N) and S the sliding distance (m). In order to estimate the volume losses correctly, the track profiles were measured with a surface profilometer (Taylor-Hobson Talysurf) which maps the surface morphology by putting a stylus in mechanical contact with the sample, being the step 0.01 μm and the scanning speed 0.1 mm/s. Profilometer was used to determine three dimensional topographic map of a surface.

3. Results and discussion

Fig. 2 shows SEM images of a fracture surface of monolithic Al_2O_3, and the Al_2O_3–SiC nanocomposites. The SiC and Al_2O_3 grains are the brighter and darker phase respectively. The nanocomposite shows SiC nanoparticles evenly distributed in the alumina matrix. The SiC particles were found both in intra- and intergranular regions, the latter being the majority. In good accord with literature, the larger SiC grains are located at grain boundaries, smaller ones are incorporated in the matrix grains.

On the other hand, Al_2O_3 grain growth at temperature as high as 1770 °C is inhibited due to these second-phase SiC particles that can be pinning grain boundaries. The monolithic alumina exhibits an equiaxed grain size matrix. The mean grain size was found to be ≈4 μm, very similar to the alumina matrix of the nanocomposite. This is important in a comparative study since grain size is known to strongly affect the wear behaviour. The relative densities of the obtained sintered nanocomposites and monolithic alumina were found to be >98% theoretical.

Table 1 gives the density, Vickers hardness (Hv), flexure strength (σ_f) and indentation fracture toughness of the monolithic alumina obtained by hot press, and nanocomposite

Table 1
Mechanical properties of alumina–silicon carbide nanocomposite and hot pressed alumina.

Composition of sample	Al_2O_3–SiC	Al_2O_3
Density (g/cm^3)	3.86 ± 0.01	3.97 ± 0.01
Vickers hardness HV1 (GPa)	21.1 ± 0.3	20 ± 0.2
Fracture toughness (MPa m$^{1/2}$)	5.4 ± 0.3	3.8 ± 0.3
Flexure strength (MPa)	551 ± 54	520 ± 13

fabricated by thermoplastic forming technologies. The fracture toughness increased with the addition of SiC particles. It should be noticed that the surface residual stresses may influence the indentation toughness measurement procedure in Al_2O_3–SiC nanocomposites which were prepared in previous works mainly using hot-pressing (HP) methods.[9] Vickers hardness of Al_2O_3 matrix was not considerably affected by the presence of SiC nanoinclusions. The flexural strength values obtained for alumina are slightly lower than that obtained for the nanocomposite material in close agreement with their lower fracture toughness value. The higher toughness value of the nanocomposite compared with the monolithic alumina with a similar grain size, can be connected with the intergranular location of the SiC submicroparticles.[2] A change in fracture mechanism has been detected, from intergranular (monolithic alumina) (Fig. 2A–C) to mixed inter (∼60% of fracture area)/transgranular (Al_2O_3/SiC nanocomposites) (Fig. 2B–D). In a monolithic alumina, the residual stresses arise at interfaces due to thermal expansion anisotropy of an alumina grain during cooling. A crack extends selecting the interfaces under the residual traction and the predominant fracture mode is intergranular.

The 3D wear track surface topography for Al_2O_3–SiC composite and hot pressed alumina after sliding against pure alumina ball is presented in Fig. 3. From the 3D wear track surface topographies, the corresponding wear track dimensions, i.e. depth and width, as well as the wear volume (W wear), were extracted for both samples, as summarized in Table 2. Under identical conditions of wear path, sliding speed and contact load, the smallest depth and width of the wear scars were measured for the alumina–silicon carbide composite, whereas the highest values are found with the hot pressed alumina. The monolithic material shows 6 times higher specific wear rate. The profile shapes and morphologies of the scars confirm that, under identical conditions of sliding distance, sliding speed and contact load, the smaller depth and width of the wear tracks are encountered with the alumina–silicon carbide composite. Examination of the materials wear surfaces confirmed that the observed changes in wear rate behaviour are related to a fundamental change in the process of wear. Fig. 4A gives an SEM micrograph of the worn surface of the nanocomposite after tribotesting. A relatively smooth region is observed. In this figure it can be observed the small particle size of the wear debris indicating that they were probably removed from the material by plastic deformation, this feature is characteristic of abrasive wear. On the contrary, the monolithic alumina worn surface generated under the same sliding conditions was generally rough (Fig. 4B). Evidence of pull out was observed. This morphology is generated by an intragranular fracture dominated material removal mechanism.

Table 2
Wear scar dimensions for Al_2O_3–SiC composites and hot pressed Al_2O_3 slid against pure alumina ball (s = 10 km, v = 0.06 m/s, F_N = 20 N).

Composition of sample	Width (μm)	Depth (μm)	W wear (mm^3/N m)
Al_2O_3–SiC	228 ± 10	3.52 ± 0.03	7.5×10^{-10}
Al_2O_3	338 ± 10	9.03 ± 0.03	4.2×10^{-9}

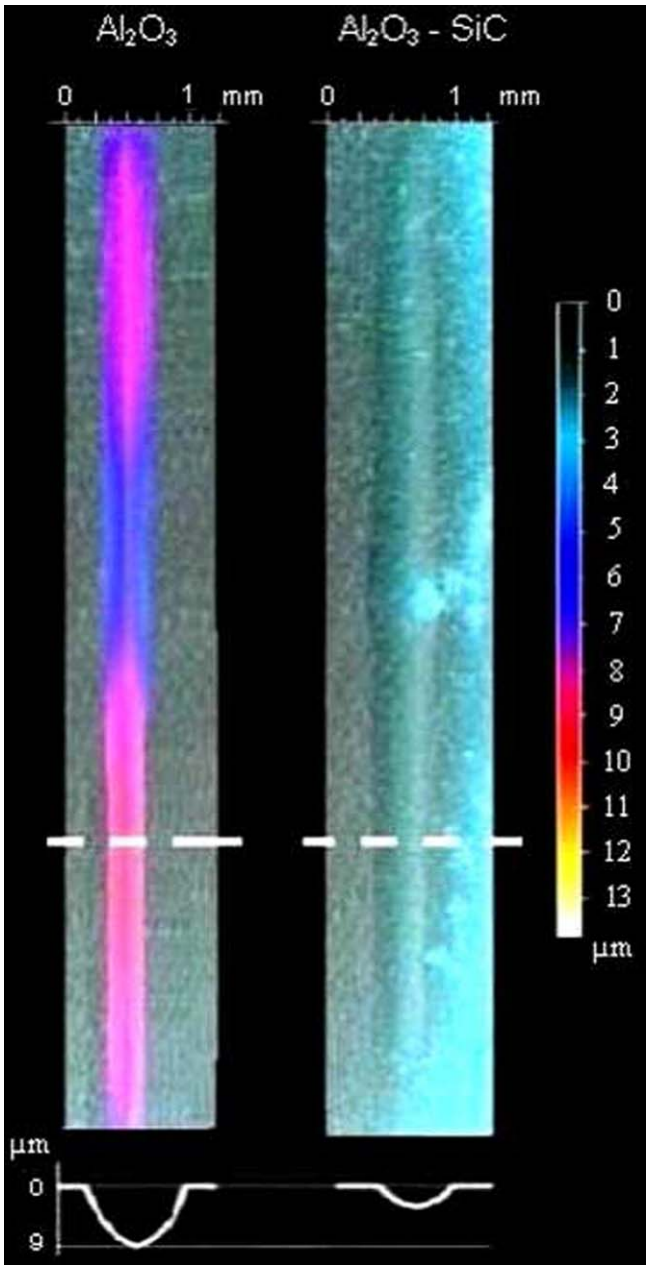

Fig. 3. 3D wear track topographies and 3D profiles of Al_2O_3–SiC nanocomposite and hot pressed alumina with width and depth scales, slid against pure alumina ball (S = 10 km, F_N = 20 N, V = 0.06 m/s).

It can be therefore stated here, that it is possible to fabricate by thermoplastic processing technologies Al_2O_3–SiC nanocom-

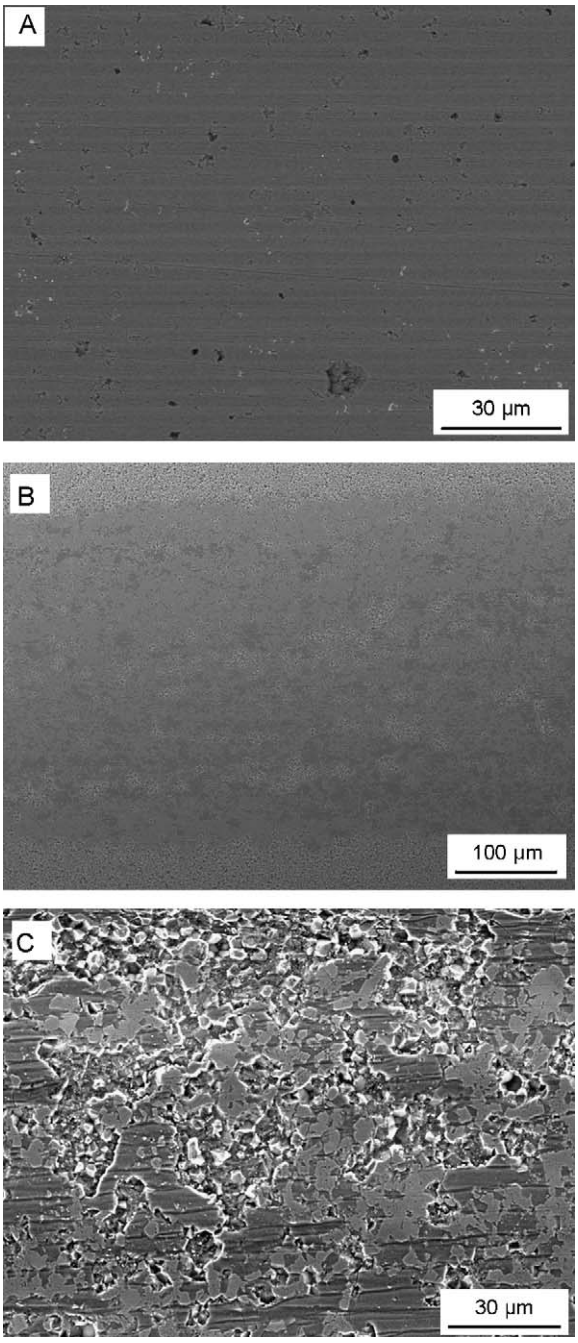

Fig. 4. SEM micrograph of the worn surface of the Al_2O_3–SiC nanocomposite (A), hot pressed alumina (B) and zone of wear track of hot pressed alumina (C) after tribotesting.

posites with very low wear rate combined with a high toughness value. The obtained values of wear resistance and toughness favourably compete with those of Al_2O_3–SiC nanocomposites fabricated by other more complex processing routes such as hot press or hot isostatic pressing.

4. Conclusions

- Al_2O_3–SiC nanocomposites were processed by ceramic injection molding (CIM). The wear rate for these nanocomposites was found to be 6 times lower than the ones corresponding to hot pressed monolithic alumina.
- The results obtained in the present investigation clearly point out that the alumina–silicon carbide nanocomposite materials obtained by reliable thermoplastic forming can be considered an excellent candidate for wear resistance components as well as for cutting tools. The flexibility of this route (in terms of the geometrical complexity of manufactured products) and its relative cost effectiveness are compelling.

Acknowledgments

This work has been supported by the Spanish Ministry of Science and Innovation under MAT2009-14542-C02-01 Project and CSIC under 200860I119 Project; Estonian Science Foundation has also supported this work under grant 8211. A. Smirnov has been funded by "DoRa" Internationalisation Programme.

References

1. Niihara K. New design concept of structural ceramics. Ceramic nanocomposites. *J Ceram Soc* 1991;**99**(10):974–82.
2. Sternitzke M. Review: structural ceramic nanocomposites. *J Eur Ceram Soc* 1997;**17**:1061–82.
3. Kovalev S, Ohji T, Yamauchi Y, Sakai M. Grain boundary strength in non-cubic ceramic polycrystals with misfitting intragranular inclusions (nanocomposites). *J Mater Sci* 2000;**35**:1405–12.
4. Davidge RW, Twigg PC, Riley FL. Effects of silicon carbide nanophase on the wet erosive wear polycrystalline alumina. *J Eur Ceram Soc* 1996;**16**:799–802.
5. Kara H, Roberts SG. Polishing, behavior and surface quality of alumina and alumina/silicon carbide nanocomposites. *J Am Ceram Soc* 2000;**83**(5):1219–25.
6. Sternitzke M, Dupas E, Twigg P, Derby B. Surface mechanical properties of alumina matrix nanocomposites. *Acta Mater* 1997;**45**:3963–73.
7. Wu H, Roberts SG, Derby B. Residual stress and subsurface damage in machined alumina and alumina/silicon carbide nanocomposites ceramics. *Acta Mater* 2001;**49**:507–17.
8. Rodriguez J, Martin A, Pastor JY, Llorca J, Bartolome JF, Moya JS. Sliding wear of alumina/silicon carbide nanocomposites. *J Am Ceram Soc* 1999;**82**(8):2252–4.
9. Zhao J, Stearns LC, Harmer MP, Chan HM, Miller GA. Mechanical-behavior of alumina–silicon carbide nanocomposites. *J Am Ceram Soc* 1993;**76**:503–10.
10. Winn AJ, Todd RI. Microstructural requirements for alumina–SiC nanocomposites. *Br Ceram Trans* 1999;**98**:219–24.
11. Walker CN, Borsa CE, Todd RI, Davidge RW, Brook RJ. Fabrication, characterisation and properties of alumina matrix nanocomposites. *Br Ceram Proc* 1994;**53**:249–64.
12. Ortiz Merino JL, Todd RI. Relationship between wear rate, surface pull-out and microstructure during abrasive wear of alumina and alumina/SiC nanocomposites. *Acta Mater* 2005;**53**:3345–57.
13. Todd RI, Limpichaipanit A. Microstructure–property relationships in wear resistant alumina/SiC "nanocomposites". *Adv Sci Technol* 2006;**45**:555–63.
14. Borsa CE, Jiao S, Todd RI, Brook RJ. Processing and properties of Al_2O_3/SiC nanocomposites. *J Microsc* 1995;**177**:305–12.
15. Sedlacek J, Galusek D, Svancarek P, Riedel R, Atkinson A, Wang X. Abrasive wear of Al_2O_3–SiC and Al_2O_3–(SiC)–C composites with micrometer- and submicrometer-sized alumina matrix grains. *J Eur Ceram Soc* 2008;**28**:2983–93.
16. Wang J, Lim SY, Ng SC, Chew CH, Gan LM. Dramatic effect of a small amount of MgO addition on the sintering of Al_2O_3–5 vol.% SiC nanocomposite. *Mater Lett* 1998;**33**:273–7.

17. Jeong Y-K, Nakahira A, Niihara K. Effects of additives on microstructure and properties of alumina–silicon carbide nanocomposites. *J Am Ceram Soc* 1999;**82**:3609–12.
18. Cock AM, Shapiro IP, Todd RI, Roberts SG. Effects of yttrium on the sintering and microstructure of alumina–silicon carbide "nanocomposites". *J Am Ceram Soc* 2005;**88**:2354–61.
19. Pillai SKC, Baron B, Pomeroy MJ, Hampshire S. Effect of oxide dopants on densification, microstructure and mechanical properties of alumina–silicon carbide nanocomposite ceramics prepared by pressureless sintering. *J Eur Ceram Soc* 2004;**24**:3317–26.
20. Shapiro IP, Todd RI, Titchmarsh JM, Roberts SG. Effects of Y_2O_3 additives and powder purity on the densification and grain boundary composition of Al_2O_3/SiC nanocomposites. *J Eur Ceram Soc* 2009;**29**:1613–24.
21. Gustafsson A, Falk LKL, Liden E, Carlstrom E. Pressureless sintered Al_2O_3–SiC nanocomposites. *Ceram Int* 2008;**34**:1609–15.
22. Miranzo P, Moya JS. Elastic/plastic indentation in ceramics: a fracture toughness determination method. *Ceram Int* 1984;**10**.
23. Bajwa S, Rainforth WM, Lee WE. Sliding wear behaviour of SiC–Al_2O_3 nanocomposites. *Wear* 2009;**259**:553–61.